MTL TR 91-27

AD-A239 560

AD

(2)

RESPONSE OF AN ALUMINA FIBER REINFORCED ALUMINUM COMPOSITE TO COMBINED TENSION-TORSION

NIKOS TSANGARAKIS, GARY P. PELLETIER, and
MARC S. PEPI
MATERIALS TESTING AND EVALUATION BRANCH

July 1991

Approved for public release; distribution unlimited.

91-08167

US ARMY
LABORATORY COMMAND
MATERIALS TECHNOLOGY LABORATORY

U.S. ARMY MATERIALS TECHNOLOGY LABORATORY
Watertown, Massachusetts 02172-0001

The findings in this report are not to be construed as an official Department of the Army position, unless so designated by other authorized documents.

Mention of any trade names or manufacturers in this report shall not be construed as advertising nor as an official indorsement or approval of such products or companies by the United States Government.

DISPOSITION INSTRUCTIONS

Destroy this report when it is no longer needed
Do not return it to the originator

UNCLASSIFIED

SECURITY CLASSIFICATION OF THIS PAGE *(When Data Entered)*

REPORT DOCUMENTATION PAGE		READ INSTRUCTIONS BEFORE COMPLETING FORM
1. REPORT NUMBER MTL TR 91-27	2. GOVT ACCESSION NO.	3. RECIPIENT'S CATALOG NUMBER
4. TITLE *(and Subtitle)* RESPONSE OF AN ALUMINA FIBER REINFORCED ALUMINUM COMPOSITE TO COMBINED TENSION-TORSION		5. TYPE OF REPORT & PERIOD COVERED Final Report 6. PERFORMING ORG. REPORT NUMBER
7. AUTHOR*(s)* Nikos Tsangarakis, Gary P. Pelletier, and Marc S. Pepi		8. CONTRACT OR GRANT NUMBER*(s)*
9. PERFORMING ORGANIZATION NAME AND ADDRESS U.S. Army Materials Technology Laboratory Watertown, Massachusetts 02172-0001 SLCMT-MRM		10. PROGRAM ELEMENT, PROJECT, TASK AREA & WORK UNIT NUMBERS D/A Project: IL162105AH42
11. CONTROLLING OFFICE NAME AND ADDRESS U.S. Army Laboratory Command 2800 Powder Mill Road Adelphi, Maryland 20783-1145		12. REPORT DATE July 1991 13. NUMBER OF PAGES 14
14. MONITORING AGENCY NAME & ADDRESS *(if different from Controlling Office)*		15. SECURITY CLASS. *(of this report)* Unclassified 15a. DECLASSIFICATION/DOWNGRADING SCHEDULE

16. DISTRIBUTION STATEMENT *(of this Report)*

Approved for public release; distribution unlimited.

17. DISTRIBUTION STATEMENT *(of the abstract entered in Block 20, if different from Report)*

18. SUPPLEMENTARY NOTES

19. KEY WORDS *(Continue on reverse side if necessary and identify by block number)*

Metal matrix	Failure envelope
Composites	Aluminum composites
Biaxial loading	Tension-Torsion

20. ABSTRACT *(Continue on reverse side if necessary and identify by block number)*

(SEE REVERSE SIDE)

DD FORM 1 JAN 73 1473 EDITION OF 1 NOV 65 IS OBSOLETE

UNCLASSIFIED

SECURITY CLASSIFICATION OF THIS PAGE *(When Data Entered)*

Block No. 20

ABSTRACT

Aluminum coupons reinforced unidirectionally with continuous alumina fibers were loaded in combined tension-torsion. Experimental results indicated that the superimposition of a 0.0025 shear strain reduced the tensile strain to failure by 67%. Similarly, the superimposition of a 0.0007 tensile strain reduced the shear strain to failure by 81%. It was inferred that applying the torque first and then the axial load or the axial load first and then the torque, had no significant effect on the failure envelope. The shear modulus was estimated to be 50.56 GPa.

INTRODUCTION

The introduction of fiber reinforced composites in structural design has generated the need to develop new test procedures for rating these materials. The assessment of the performance of such composites under combined tensile-torsional loading should increase their reliability. Specimens such as the cruciform,[1-4] the thin wall cylinder,[5-11] and the center cracked plate[12] have been used extensively to investigate the response of isotropic materials to biaxial loading. These specimens, however, may not be appropriate for all types of fiber reinforced composites. It has been shown that, in certain composites, premature failure by fiber debonding can occur at points of stress concentration or where there is a change in the specimen's contours.[13,14] Because of these trends, the cruciform and the center cracked plate could be poor candidates for combined tensile-torsional testing of fiber reinforced composites, especially those reinforced unidirectionally. On the other hand, the thin wall cylindrical specimen could be promising for certain applications (e.g. pressure vessels) provided that the cost of producing it or its availability are not problematic.

The above considerations have led the authors to select a simple bar with a narrow rectangular cross section as a suitable specimen for combined axial-torsional testing of a fiber reinforced composite. The specimen configuration and dimensions are depicted in Figure 1. The ends of the coupon were protected with aluminum tabs. When a coupon with a narrow rectangular cross section is loaded in pure torsion as shown in Figure 2, the total shear strain γ_{zy} of the element "abcd" consists of two components. The first component is the shear strain $\gamma_1 = \zeta_v / \zeta_z$ (rotational shear strain) which is due to the rotation of the cross section about the "z" axis and the second component is the shear strain $\gamma_2 = \zeta_w / \zeta_y$ which is due to warpage of the cross section. For isotropic materials $\gamma_1 = \gamma_2$, and the resultant shear is twice as great as in the case of a circular cross section of diameter "2a".[15] For an orthotropic solid, the shear strain γ_{zy} in the middle portion of the long side of the coupon is:

$$\gamma_{zy} = \zeta_v / \zeta_z + \zeta_w / \zeta_y = \theta \cdot a + \zeta_w / \zeta_y \qquad (1)$$

where "θ" is the angle of rotation per unit gage length and "a" is half the coupon's thickness. In the present study, the shear strain γ_{zy} is monitored with strain gages and the warpage is obtained from Equation 1. Axial tensile strains are monitored with an axial strain gage. The response of the composite under such combined loading is analyzed.

MATERIAL AND EXPERIMENTAL PROCEDURE

Continuous alumina fiber reinforced aluminum composite (FP/Al) coupons (1.27 cm x 0.25 cm x 15.25 cm) were prepared from a liquid-infiltrated as-cast plate which was manufactured by DuPont.[16] An Al-2.5% Li (6061-T6) alloy was used as the matrix material by the manufacturer to promote bonding between the alumina fibers and the matrix alloy. The composite contained 55% fiber by volume which was unidirectional and oriented parallel to the coupon's length. The uniaxial properties of the composite have been examined earlier.[17] These composite properties are listed in Table 1. Typical filament physical properties are given in Table 2.

Combined tensile-torsional tests were conducted in a 2,260 N-m torsional and 180 KN axial capacities MTS servohydraulic machine. Serrated hydraulic grips were used to hold the test coupons. The specimens had their ends protected from the serrations of the hydraulic grips with aluminum tabs which were 2 mm thick. The length of the aluminum tabs was 51 mm, thus the coupons' gage length was 51 mm. Axial strains, e_{zz}, were monitored with a single

longitudinally oriented strain gage. This strain gage was positioned 2 cm from the edge of one of the aluminum tabs and at the center of the long specimen's side. The output of a Wheatstone bridge, with two active shear gages (at ±45° relative to the specimen's longitudinal axis) was used to monitor the shear strains. The location of the strain gages is shown in Figure 1. When the shear gages were connected on adjacent bridge sites, the output of this bridge was:

$$Vo = Vi \cdot GF \cdot \gamma_{zy} / 4 \qquad (2)$$

where Vi is the bridge input voltage, and GF is the gage factor. The shear strain γ_{zy} was estimated from Equation 2. This strain was maximal along the center portion of the long sides of the coupon. The amount of warpage was found by subtracting "θa" (2a = 0.25 cm) from γ_{zy}. The value of "θ" was obtained as the ratio of the angle of rotation (test machine's output) divided by the coupon's gage length.

Table 1. COMPOSITE MECHANICAL PROPERTIES

$E_{xx} = E_{yy} = 138$ GPa
$E_{zz} = 210$ GPa
$\nu_{zy} = \nu_{zx} = 0.26 - 0.31$
UTS = 543 - 589 MPa
$e_f = 0.003$

NOTE: E_{ii} = elastic constants
ν_{zi} = Poisson's ratios
UTS = ultimate tensile stress
e_f = axial tensile fracture strain

Table 2. ALUMINA CONTINUOUS FIBER PROPERTIES

Elastic Modulus = 380 GPa
Ultimate Tensile Strength = 1,380 MPa
Diameter = 20 um
Density = 3.9 g/cm^3

In order to validate a test, the four types of eccentricity shown in Figure 3 had to be minimized. A straight steel rod, which was used to install the hydraulic grips in the MTS machine, was also used to minimize the first two types of eccentricity. This was accomplished by applying a 20 N-m torque to the steel rod prior to the final fastening of the grips. This torque caused the grips to self-adjust which minimized the first two eccentricities. A bubble leveling tool and the grips' center markings were found helpful to minimize the last two types of eccentricity. After a coupon was positioned in the grips, loads were applied in two steps. First, the coupon was torqued or pulled in tension and then a tensile load or a torque was superimposed, respectively. Torsional loading was under rotational control (not torque control).

During loading, torques; axial loads, and the angle of rotation were monitored directly from the circuitry of the MTS test machine. Shear and axial strains were obtained from the strain gages which were attached onto the coupons.

Metalographic examination of tested coupons was conducted to determine the features of the fracture surfaces. The surface portion of the matrix material was leached away with dilute hydrochloric acid in the gage section of selected tested coupons. The number of fiber breaks and their distribution across the gage length was then assessed microscopically.

EXPERIMENTAL RESULTS AND DISCUSSION

The composite's response to pure torsional loading is represented by the curve closest to the ordinate in Figure 4. Yielding initiated at a torque of 0.9 N-m, which was related to a rotational sheer strain (γ_1) of 0.00033. The shear strain component γ_2, which represents the maximal amount of warpage, was found to be not equal to γ_1. Experimental results indicated that for both linear elastic and elastic-plastic deformations: $\gamma_2 = 1.22 \cdot \gamma_1$. Therefore, it is inferred that there was an orthotropic effect on the relative magnitudes of γ_1 and γ_2. Thus, the total shear strain ($\gamma_1 + \gamma_2$) at the elastic limit of the first curve of Figure 4 was 0.00072. Assuming the membrane analogy model[15] valid, from Equation 3 the shear modulus G_{zy} is 50.56 GPa.

$$T = G_{zy} \cdot \theta \cdot 2b \cdot (2a)^3 / 3 \qquad (3)$$

where "T" is the applied torque and 2b = 1.27 cm.

A similar approach was used by Kurtz and Sun[18] for the determination of the shear modulus of an orthotropic composite. The total (elastic plus plastic) rotational shear strain to failure was 0.0206 excluding warpage or 0.0453 including warpage. The middle curve of Figure 4 represents the composite's response to combined torsional-tensile loading. This coupon was first torqued to a rotational shear strain 0.013 and then loaded in tension to failure. The tensile stress-strain relationship was linearly elastic with a slope of 210 GPa. This modulus value is typical for this composite when loaded uniaxially in tension. The tensile strain at failure was 0.00062. It was noted that during the application of the tensile load the torque initially decreased slowly from 4.176 N-m to 2.848 N-m and then to zero in a catastrophic manner. The rotational shear strain, however, was held constant. This implies that the torque decrease could be due to a relief in warpage loading by shearing of the matrix in a direction which was parallel to the fibers, fibers debonding, or both matrix shearing and fibers debonding. Note the two decreases in torque at rotational shear strains 0.0068 and 0.011, respectively. These two torque decreases could be indicative of some fiber fracture, matrix cracking, or fiber debonding. The last curve in Figure 4 is the composite's response to an axial tensile strain of 0.0005 which was followed by a superimposed rotational shear strain to failure 0.012. The tensile loading was linearly elastic with a slope of 210 GPa which is typical for this composite.[17] During torsion the applied tensile load had to be reduced to zero so that the tensile strain (as indicated by the coupon's strain gage) remained constant (0.0005). Note that at a rotational shear strain of 0.0041, the torque decreased from 3.16 N-m to 2.44 N-m. This torque decrease could be indicative of some composite damage. Two additional minor torque decreases are also noted near the end of the shear loading prior to catastrophic failure of the coupon. Results from this test as well as from other tests indicated that the shear

otational strain for yielding initiation remained unaffected from the superimposed tensile train. The shear moduli obtained from the last two curves were of the same value as that f the first curve.

Coupon failures under combined torsional-axial tensile monotonic loading are depicted in igure 5. The shear rotational strain component ($\gamma_1 = \theta \cdot a$) is the abscissa and the axial tenile strain, e_{zz}, is the ordinate. The open circles indicate that tensile loading preceded torsion nd the solid circles indicate that torsion preceded tension. The dashed line approximates the ailure envelope. It is inferred from these data that the effect of the loading sequence on he failure envelope is rather insignificant. The pure rotational strain to failure was 0.0206 0.045 including warpage). However, the superimposition of an axial tensile strain 0.0007 aused an 81% reduction of the pure rotational shear strain for failure. Similarly, the supermposition of a relatively small rotational shear strain 0.0025 (0.0055 including warpage) aused a 67% reduction of the axial tensile strain at failure (0.003).

The parametric representation of the failure envelope (dashed line) of Figure 5 is:

$$\left(\frac{\gamma_1}{0.02}\right)^{0.6} + \left(\frac{e_{zz}}{0.003}\right)^{0.6} = 1 \qquad (4)$$

where "γ_1" is the shear strain and "e_{zz}" is the tensile strain. Note that in the above equation he rotational shear strain has been used and not the total strain which includes the warpage. If one wants to include the warpage in the shear strain, then Equation 4 becomes:

$$\left(\frac{\gamma_{zy}}{0.045}\right)^{0.6} + \left(\frac{e_{zz}}{0.003}\right)^{0.6} = 1 \qquad (5)$$

The plane represented by Equation 4 or Equation 5 was named by Brown and Miller[19] he "T-plane" (see Figure 5). Brown and Miller tested tubular specimens of AISI 316 stainless steel in combined tension-torsion. Using strains instead of stresses, the solid curve in Figure 5 represents the failure envelope using the Hill-Tsai failure criterion. The latter envelope is very conservative when compared to the envelope obtained from the experimental data.

The majority of the coupons' failures occurred within their gage lengths and near the upper stationary grip. The fracture surface of the coupon corresponding to the middle curve of Figure 4 is shown in Figure 6a. A crack through the coupon's thickness can be seen in the middle of the projected fracture surface (SEM photograph). The surface of this crack is parallel to the longitudinal axis of the coupon. In the authors' opinion this crack was formed under pure shear loading and is related to the two torque decreases at shear strains of 0.0068 and 0.011 (see middle curve of Figure 4). If this hypothesis is correct, the failure envelope depicted in Figure 5 should be shifted to lesser shear strains since significant composite damage could have occurred prior to catastrophic failure (fracture). The fracture surface on either side of the above crack was rough, with step-like features and with occasional debonded, broken fibers. Similar observations can be made for the fracture surface of the coupon of the last curve of Figure 4. This surface is shown in Figure 6b. The through-thickness crack in the middle of the projected fracture surface probably relates to the torque decrease at rotational shear strain of 0.0041. As discussed earlier, if failure of the coupon is defined to occur when such a crack (or torque decrease) forms, the failure envelope should be shifted to lesser shear strains. The surface roughness was similar to that of the previous

coupon with occasional debonded fibers. The latter features are shown in Figure 7. In this figure one can distinguish a secondary shear crack shown by an arrow as "b" and which is perpendicular to the primary crack noted by an arrow as "a". In the center, an area can be seen where the fibers were well bonded with the matrix. On the contrary, the areas to the left and to the right indicate fiber pullouts which are indicative of a poor matrix-fiber bonding.

The microscopic examination of several tested coupons which had their surface matrix material leached away with acid did not find any localities with a high concentration of fiber breaks. The density of fiber breaks was uniform across the entire width (long sides of the coupons) and gage area of each of the examined coupons.

The maximum torque for maintaining purely elastic deformation was found to be 0.9 N-m. This torque value corresponded to a maximal shear stress τ_{zy} of 37 MPa (from Equation 6)[15] and a total (warpage + rotational) elastic shear strain of 0.00072.

$$\tau_{zy},\ \max = G_{zy} \cdot \gamma_{zy} \tag{6}$$

For higher torque values, plastic shear deformation should initiate at the surface of the long sides of the coupon and spread inward toward the coupon's center. The distribution of Z_{zy} along half a long side of the coupon, assuming elastic deformation only, is depicted in Figure 8. This distribution was obtained from a numerical evaluation of Equation 7 which was derived using the membrane analogy model and is provided by Timoshenko:[15]

$$\tau_{zy} = \frac{16}{\pi^2} \cdot G_{zy} \cdot \theta \cdot a \cdot \sum_{\eta=1,3,5\ldots}^{\infty} \left\{ \frac{1}{\eta^2} \cdot (-1)^{\frac{\eta-1}{2}} \cdot \left(1 - \frac{\cosh \frac{\eta \pi y}{2a}}{\cosh \frac{\eta \pi b}{2a}} \right) \cdot \sin \left(\frac{\eta \pi x}{2a} \right) \right\} \tag{7}$$

It can be shown from Equation 7 that τ_{zy} and consequently γ_{zy} remain maximal and nearly constant within $y = \pm 2b/5$. This constancy implies that plasticity should initiate within the entire $y = \pm 2b/5$ interval and not restricted to $y = 0$. Similarly, the through-thickness cracks shown in Figure 6 could form within the same interval and should not be thought to be confined to form at $y = 0$. The observed uniformity of the distribution of the number of broken fibers along the "y" direction, which was discussed earlier, also supports the hypothesis of this type of failure. In fact, cracks like those of Figure 6 were observed to form off the long coupons' sides' centers prior to catastrophic failure of the coupons. Because of the geometry and orientation of these cracks, they are either Mode II or Mode III type. Their formation was encouraged by the unidirectionality of the composite's reinforcement. Thus, the roughness of the fracture surface of the tested coupons was the result of successive combinations of shear crack jumps and tensile failures (where appropriate). The tensile failures were accompanied by fiber pullouts (see Figure 7). The latter indicate a poor fiber-to-matrix bond.

CONCLUSIONS

The shear modulus G_{zy} of a FP/Al composite was estimated from coupons with a narrow rectangular cross section and was found to be 50.56 GPa. The failure envelope under combined torsional-axial tensile loading was not affected significantly by the loading sequence. The rotational elastic shear strain limit was 0.00033. Plastic deformation of the metal matrix initiated at an approximate shear stress value of 37 MPa. This value of the maximal shear

tress for yield initiation contains the contribution of elastic warpage of the coupons. Unlike sotropic materials, experimental results for this orthotropic material indicated that the extent of warpage was greater than the rotational shear strain component of ζ_v / ζ_z. The superimposition of a minimal shear loading significantly reduced the tensile strain to failure. A superimposed 0.0025 rotational shear strain caused a 67% decrease of the tensile strain to failure. Similarly, the superimposition of an axial tensile strain 0.0007 caused an 81% reduction of the pure rotational shear strain for composite failure. The latter strain was 0.0206.

REFERENCES

1. CHARVAT, M. H., and GARRETT, G. G. *The Development of a Closed-Loop, Servo-Hydraulic Test System for Direct Stress Monotonic and Cyclic Crack Propagation Studies under Biaxial Loading.* J. Testing and Evaluation, v. 8, no. 1, January 1980, p. 9-17.
2. PARSONS, M. W., and PASCOE, K. J. *Development of a Biaxial Fatigue Testing Rig.* J. Strain Analysis, v. 10, no. 1, 1975, p. 1-9.
3. PARSONS, M. W., and PASCOE, K. J. *Observations of Surface Deformation, Crack Initiation and Crack Growth in Low-Cycle Fatigue under Biaxial Stress.* Materials Sci. and Engng., v. 22, 1976, p. 31-50.
4. PARSONS, M. W., and PASCOE, K. J. *Low-Cycle Fatigue under Biaxial Stress.* Proc. Instn. Mech. Engrs., v. 188, no. 61/74, 1974, p. 657-671.
5. LOHR, R. D., and ELLISON, E. G. *Biaxial High Strain Fatigue Testing of 1 Cr-Mo-V Steel.* Fatigue of Engng. Mat. and Struct., v. 3, 1980, p. 19-37.
6. BROWN, M. W., and MILLER, K. J. *Biaxial Cyclic Deformation Behavior of Steels.* Fatigue of Engng. Mat. and Struct., v. 1, 1979, p. 93-106.
7. BROWN, M. W., and MILLER, K. J. *High Temperature Low Cycle Biaxial Fatigue of Two Steels.* Fatigue of Engng. Mat. and Struct., v. 1, 1979, p. 217-229.
8. HUA, C. T., and SOCIE D. F. *Fatigue Damage in 1045 Steel under Constant Amplitude Biaxial Loading.* Fatigue of Engng. Mat. and Struct., v. 7, no. 3, 1984, p. 165-179.
9. TANAKA, K., MATSUOKA, S., and KIMURA, M. *Fatigue Strength of 7075-T6 Aluminum Alloy under Combined Axial Loading and Torsion.* Fatigue of Engng. Mat. and Struct., v. 7, no. 3, 1984, p. 195-211.
10. SAUNDERS, I., and NUTTING, J. *Deformation of Metals to High Strains using Combination of Torsion and Compression.* Metal Science, v. 18, December 1984, p. 571-575.
11. SOCIE, D. F., and SHIELD, T. W. *Mean Stress Effects in Biaxial Fatigue of Inconel 718.* J. of Engng. Mat. Technology, v. 106, July 1984, p. 227-232.
12. OLADIMEJI, M. K. *Plane-Stress Fracture Testing of Finite Sheets under Biaxial Loads.* Exper. Mechanics, v. 23, no. 2, 1983, p. 217-227.
13. TSANGARAKIS, N. *The Notch-Fatigue Behavior of an Aluminum Composite Reinforced Unidirectionally with Silicon Carbide Fiber.* J. of Composite Materials, v. 21, no. 11, November 1987, p. 1008-1016.
14. TSANGARAKIS, N., ANDREWS, B. O., and CAVALLARO, C. *Mechanical Properties of Some Silicon Carbide Reinforced Aluminum Composites.* J. of Composite Materials, v. 21, no. 5, 1987, p. 481-492.
15. TIMOSHENKO, S. *Theory of Elasticity.* McGraw-Hill Book Co., Inc., New York and London, First Edition, 1934.
16. CHAMPION, A. R., et al. *Proceedings of International Conference on Composite Materials.* B. Norton et al, Eds., Metallurgical Society of the American Institute of Mining, Metallurgical and Petroleum Engineers, 1978, p. 883-904.
17. TSANGARAKIS, N., SLEPETZ, J. M., and NUNES, J. *Fatigue Behavior of Alumina Fiber Reinforced Aluminum Composites.* ASTM STP 864, 1985, p. 131-152.
18. KURTZ, R. D., and SUN, C. T. *Composite Shear Modulus from Torsion of Thick Laminates.* ASTM STP 1059, 1990, p. 508-520.
19. BROWN, M. W., and MILLER, V. J. *High Temperature Low Cycle Biaxial Fatigue of Two Steels.* Fatigue of Engng. Mat. and Struct., 1979, p. 217-229.

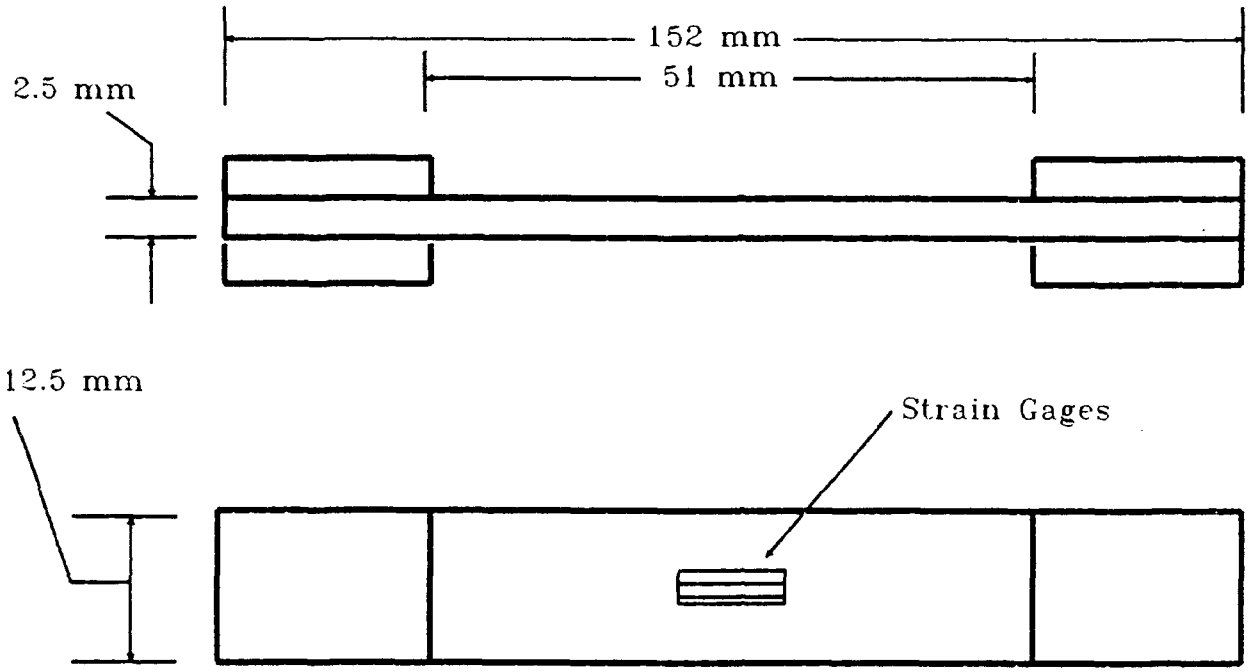

Figure 1. Specimen configuration and strain gage location.

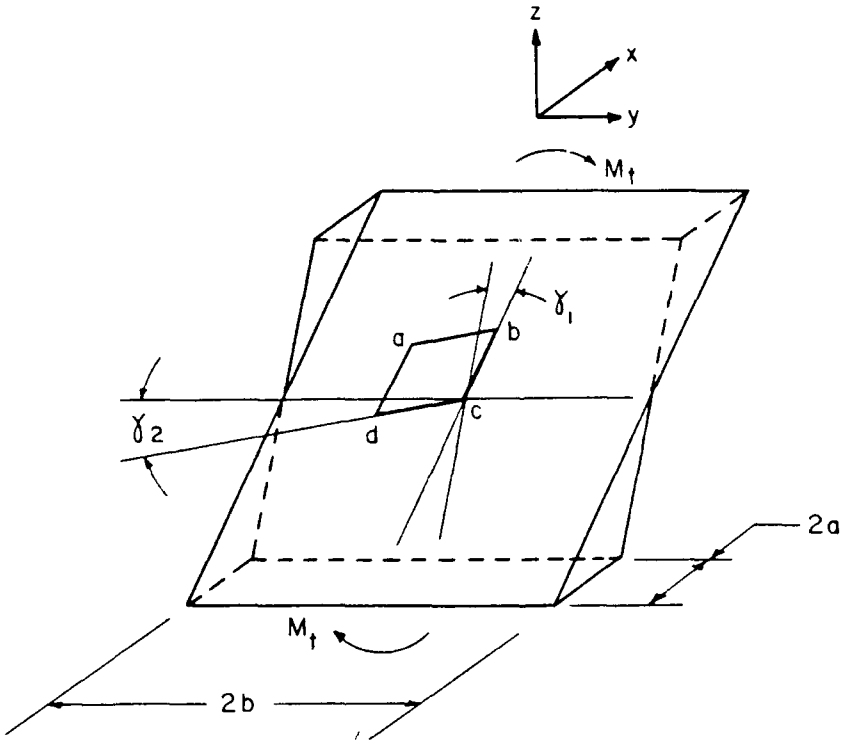

Figure 2. A bar with a rectangular cross section loaded in torsion.

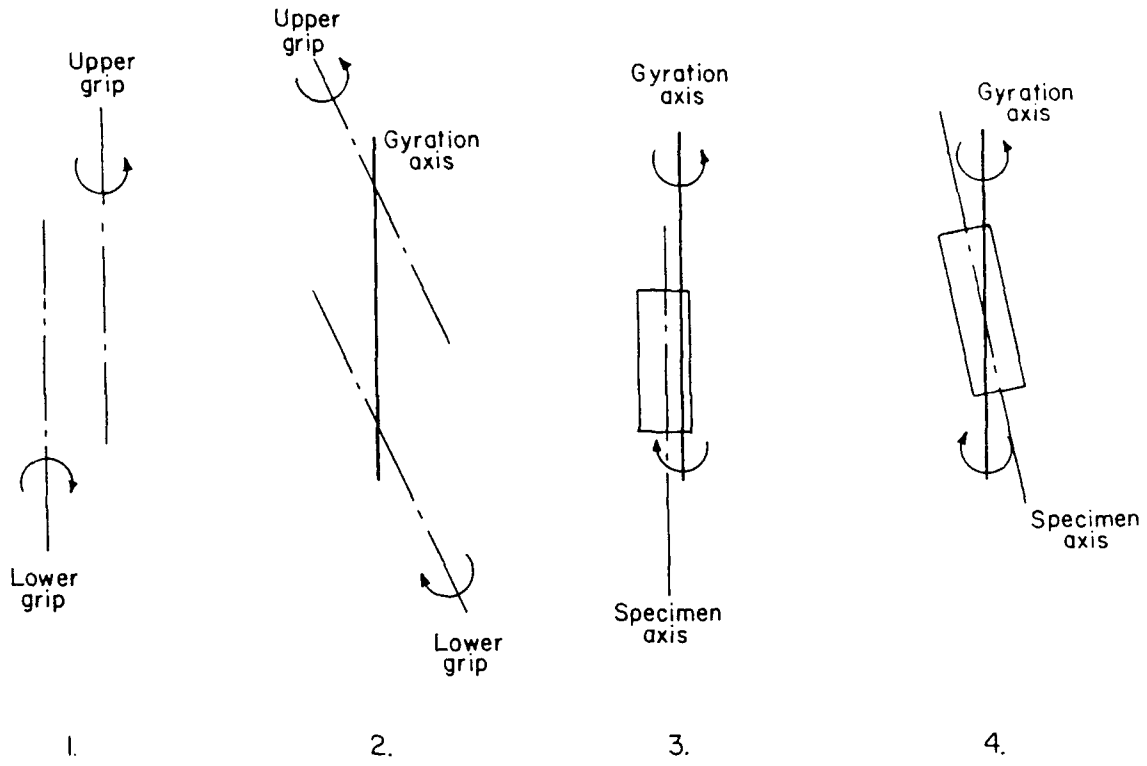

Figure 3. Types of eccentricity.

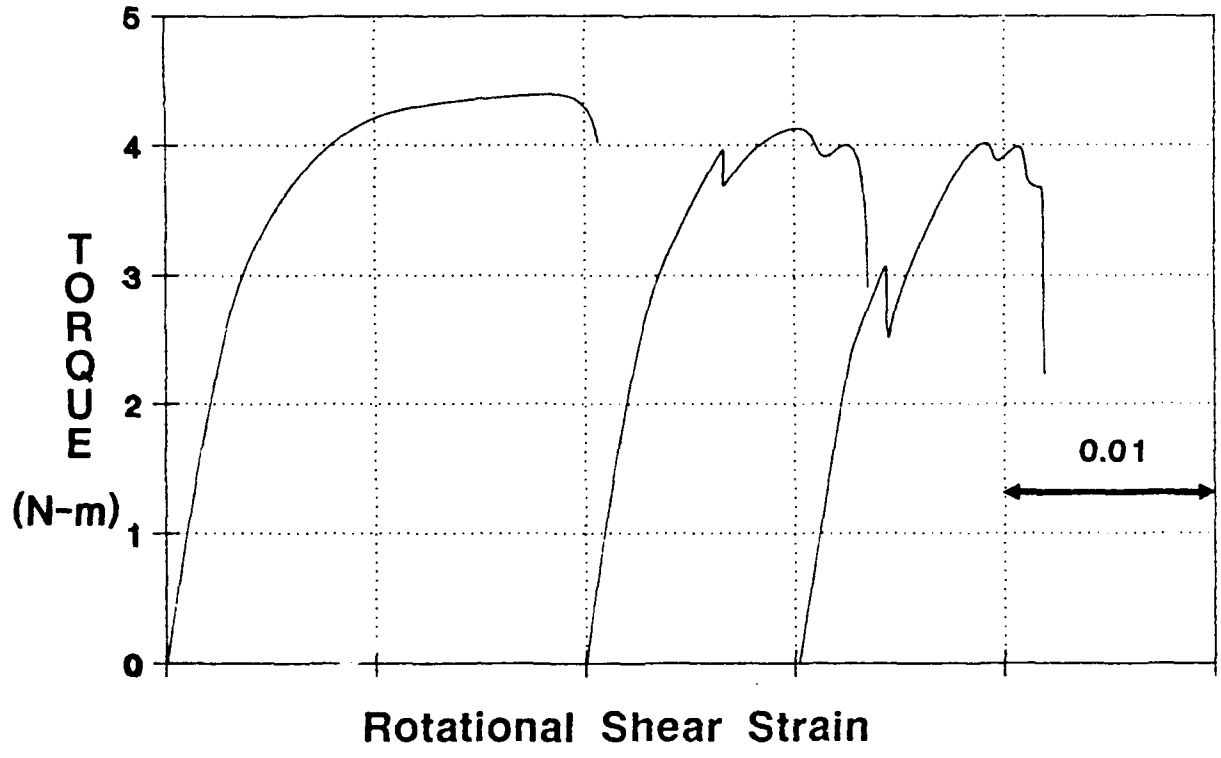

Figure 4. Composite response to combined loading.

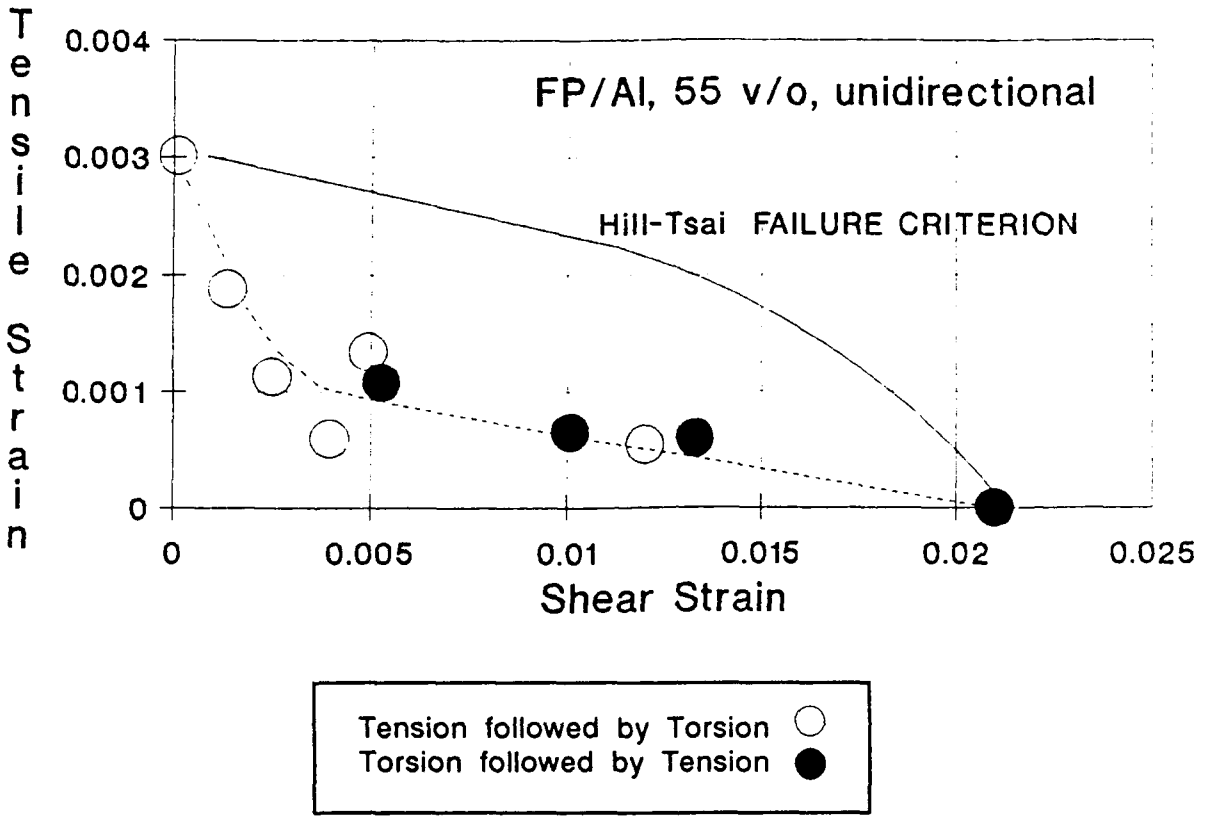

Figure 5. Failure envelope under combined tension-torsion.

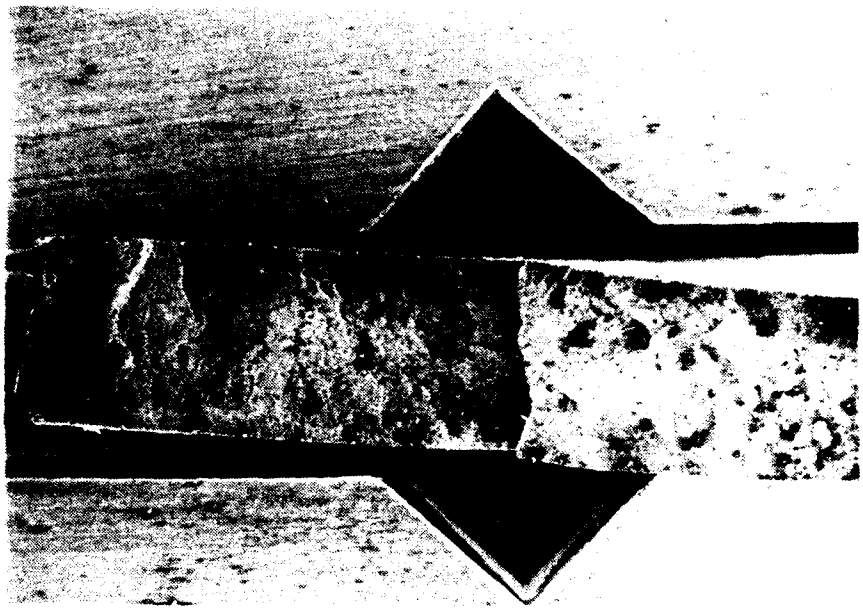

Figure 6a. Fracture surfaces.
Torsion followed by tension.

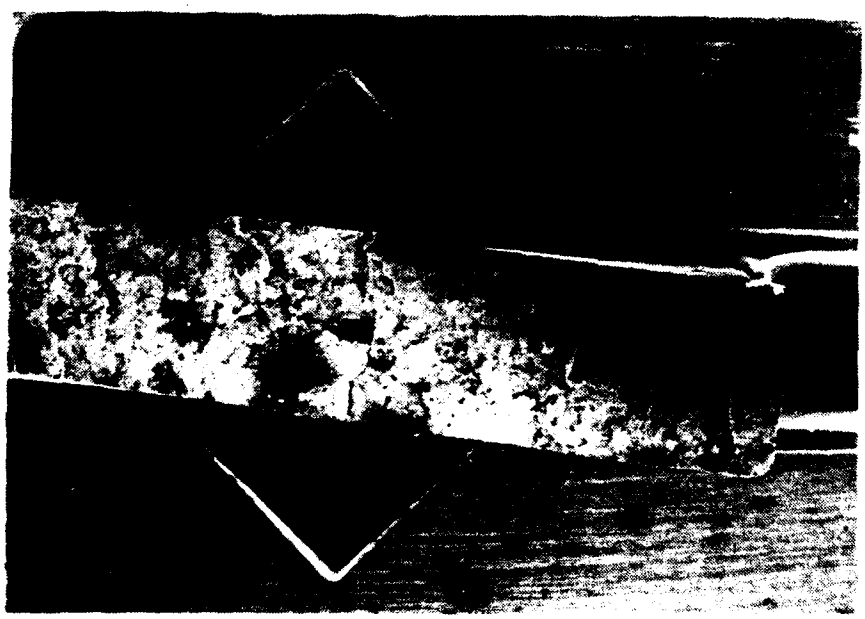

Figure 6b. Fracture surfaces.
Tension followed by torsion.

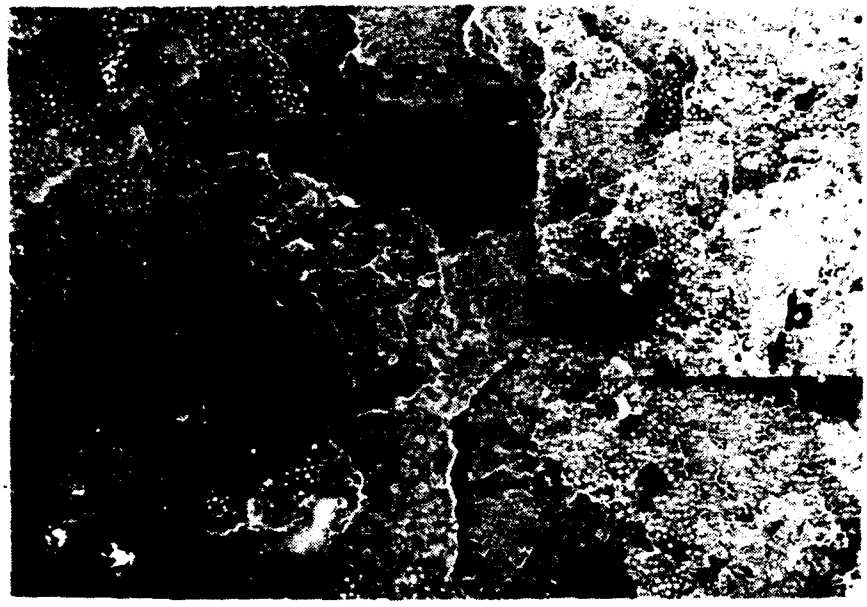

Figure 7. Fracture surface details.

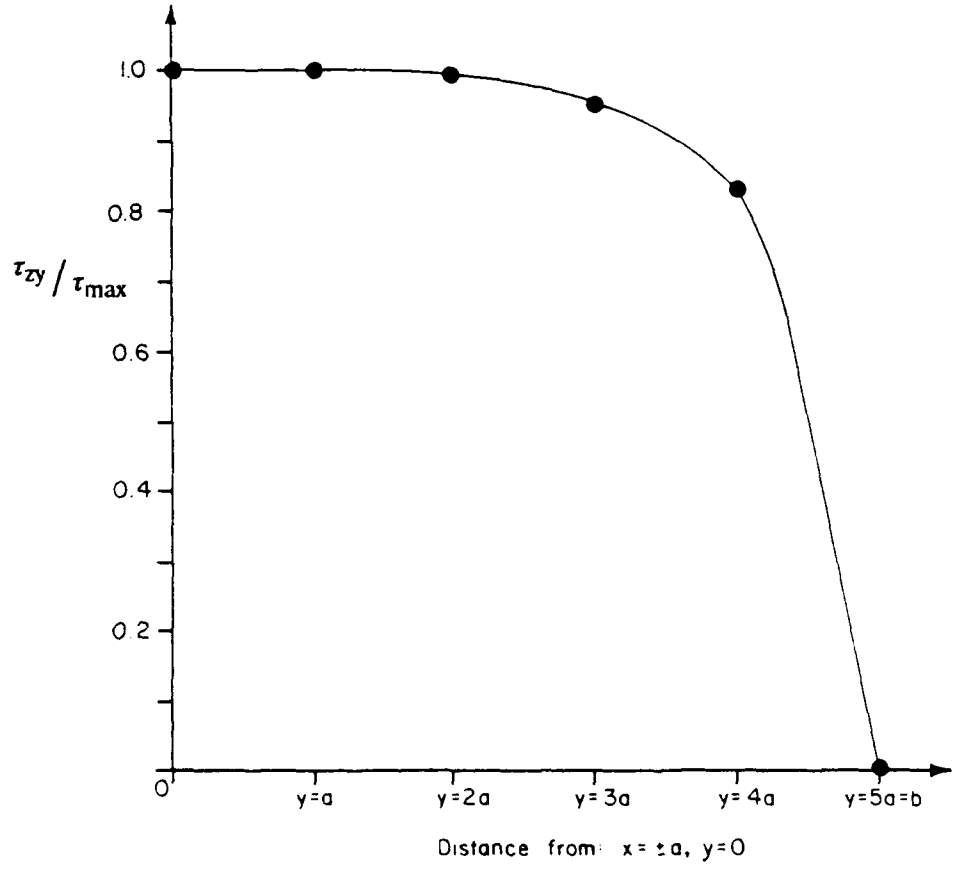

Figure 8. Elastic shear stress τ_{zy} distribution.

DISTRIBUTION LIST

No. of Copies	To
1	Office of the Under Secretary of Defense for Research and Engineering, The Pentagon, Washington, DC 20301
	Commander, U.S. Army Laboratory Command, 2800 Powder Mill Road, Adelphi, MD 20783-1145
1	ATTN: AMSLC-IM-TL
1	AMSLC-CT
	Commander, Defense Technical Information Center, Cameron Station, Building 5, 5010 Duke Street, Alexandria, VA 22304-6145
2	ATTN: DTIC-FDAC
1	MIAC/CINDAS, Purdue University, 2595 Yeager Road, West Lafayette, IN 47905
1	Defense Advanced Research Projects Agency, Defense Sciences Office/MSD, 1400 Wilson Boulevard, Arlington, VA 22209
	Headquarters, Department of the Army, Washington, DC 20314
1	ATTN: DAEN-RDM, Mr. J. J. Healy
	Commander, U.S. Air Force Wright Research & Development Center, Wright-Patterson Air Force Base, OH 45433-6523
1	ATTN: WRDC/MLLP, D. M. Forney, Jr.
1	WRDC/MLBC, Mr. Stanley Schulman
1	WRDC/MLLS, Dr. Terence M. F. Ronald
1	Edward J. Morrissey, WRDC/MLTE, Wright-Patterson AFB, OH 45433-6523
	Commander, Army Research Office, P.O. Box 12211, Research Triangle Park, NC 27709-2211
1	ATTN: Information Processing Office
	Commander, U.S. Army Materiel Command, 5001 Eisenhower Avenue, Alexandria, VA 22333
1	ATTN: AMCSCI
	Commander, U.S. Army Aviation Systems Command, 4300 Goodfellow Blvd., St. Louis, MO 63120-1798
1	ATTN: AMSAV-GTD
1	AMSAV-E
1	AMCPEO-AV
	Director, U.S. Army Ballistic Research Laboratory, Aberdeen Proving Ground, MD 21005
1	ATTN: SLCBR-TSB-S (STINFO)
	Commander, U.S. Army Foreign Science and Technology Center, 220 7th Street, N.E., Charlottesville, VA 22901-5396
3	ATTN: AIFRTC, Applied Technologies Branch, Gerald Schlesinger
	Commander, U.S. Army Materiel Systems Analysis Activity, Aberdeen Proving Ground, MD 21005
1	ATTN: AMXSY-MP, Director
	Commander, U.S. Army Missile Command, Redstone Scientific Information Center, Redstone Arsenal, AL 35898-5241
1	ATTN: AMSMI-RD-CS-R/Doc
1	AMSMI-RLM
	Commander, U.S. Army Aviation Systems Command, Aviation Research and Technology Activity, Aviation Applied Technology Directorate, Fort Eustis, VA 23604-5577
1	ATTN: SAVRT-TY-ATP, Mr. James Gomez, Aerospace Engineer
	Commander, U.S. Army Tank-Automotive Command, Warren, MI 48397-5000
1	ATTN: AMSTA-RCKM

No. of Copies	To
	Director, Benet Weapons Laboratory, LCWSL, USA AMCOM, Watervliet, NY 12189
1	ATTN: AMSMC-LCB-TL
1	AMSMC-LCB-PS, Dr. I. Ahmad
	David Taylor Naval Ship Research and Development Center, Annapolis, MD 21402
1	ATTN: Dr. Michael Vassilaros - Code 2814
	Naval Research Laboratory, Washington, DC 20375
1	ATTN: Code 5830
1	Dr. G. R. Yoder - Code 6384
1	Dr. S. C. Sanday - Code 6370
	Chief of Naval Research, Arlington, VA 22217
1	ATTN: Code 471
1	Dr. Steven G. Fishman
	Naval Sea Systems Command, Washington, DC 20362
1	ATTN: Mr. Marlin Kinna - 62R4
	Naval Air Development Center, Warminster, PA 18974
1	ATTN: Dr. E. U. Lee - Code 60632
	Naval Surface Warfare Center, White Oak, Silver Spring, MD 20910
1	ATTN: John V. Foltz - Code R32
1	Dr. Herbert Newborn - Code R34
	NASA - Washington, DC 20546
1	ATTN: Mr. Michael A. Greenfield, Program Manager for Materials, Code RTM-6
	NASA - Lewis Research Center, Cleveland, OH 44135
1	ATTN: Dr. James A. DiCarlo, Mail Stop 106-1
	NASA - Marshall Space Flight Center, MSFC, AL 35812
1	ATTN: Mr. Paul Schuerer, EH01
	The Boeing Vertol Company, P.O. Box 16858, Philadelphia, PA 19142
1	ATTN: Mr. Robert L. Pinckney, Mail Stop P62-06
1	Mr. Joseph W. Lenski, Jr., Mail Stop P32-09
	E. I. DuPont De Nemours and Company, Inc., Textile Fibers Department, Pioneering Research Laboratory, Experimental Station, Wilmington, DE 19898
1	ATTN: Blake R. Bichlmeir
1	Mr. Rex C. Claridge, TRW, Incorporated, Manufacturing Division, Mail Stop 01-2210, 1 Space Park, Redondo Beach, CA 90278
1	Dr. James A. Cornie, Materials Processing Center, Bldg. 8, Room 237, Massachusetts Institute of Technology, 77 Massachusetts Avenue, Cambridge, MA 01239
1	Dr. Bhagwam K. Das, Engineering Technology Supervisor, The Boeing Company, P.O. Box 3999, Seattle, WA 98124
1	Leroy Davis, NETCO, 592 Dryad Road, Santa Monica, CA 9042-1318
1	Mr. Joseph F. Dolowy, Jr., President, DWA Composite Specialties, Inc., 21133 Superior Street, Chatsworth, CA 91311
1	Mr. Robert E. Fisher, President, AMERCOM, Inc., 8948 Fullbright Avenue, Chatsworth, CA 91311
1	Prof. James G. Goree, Dept. of Mechanical Engineering, Clemson University, Clemson, SC 29631
1	William F. Grant, AVCO Specialty Materials Division, 2 Industrial Avenue, Lowell, MA 01851
1	Mr. Jacob Gubbay, Charles Stark Draper Laboratories, 555 Technology Square, Mail Station 27, Cambridge, MA 02139

No. of Copies	To
1	Dr. H. A. Katzman, The Aerospace Corporation, P.O. Box 92957 Los Angeles, CA 90009
	Lockheed Georgia Company, 86 South Cobb Drive, Marietta, GA 30063
1	ATTN: Materials and Processes Engineering Department
1	Mr. James Carroll
	Materials Concepts, Inc., 666 Hague Avenue, Columbus, OH 43204
1	ATTN: Mr. Stan J. Paprocki
1	Mr. David Goddard
1	Dr. Mohan S. Misra, Martin Marietta Aerospace, P.O. Box 179, Denver, CO 80201
1	Mr. Patrick J. Moore, Staff Engineer, Lockheed Missiles and Space Company, Organization 62-60, Building 104, P.O. Box 504, Sunnyvale, CA 94086
1	R. Byron Pipes, Professor & Director, Center for Composite Materials, University of Delaware, Newark, DE 19711
1	Dr. Karl M. Prewo, Principal Scientist, United Technologies Research Center, Mail Stop 24, East Hartford, CT 06108
1	Dr. B. W. Rosen, Materials Sciences Corporation, 930 Harvest Drive, Suite 300, Blue Bell, PA 19422
1	Prof. Marc H. Richman, Division of Engineering, Brown University, Providence, RI 02912
1	Mr. Ronald P. Tye, Energy Materials Testing Laboratory, Biddeford Industrial Park, Biddeford, ME 04005
1	Prof. Franklin E. Wawner, Department of Materials Science, School of Engineering and Applied Sciences, University of Virginia, Charlottesville, VA 22903
1	Dr. Carl Zweben, General Electric Company, Valley Forge Space Center/M4018, P.O.Box 8555, Philadelphia, PA 19101
	Director, U.S. Army Materials Technology Laboratory, Watertown, MA 02172-0001
2	ATTN: SLCMT-TML
3	Authors

U.S. Army Materials Technology Laboratory
Watertown, Massachusetts 02172-0001
RESPONSE OF AN ALUMINA FIBER REINFORCED ALUMINUM COMPOSITE TO COMBINED TENSION-TORSION -
Nikos Tsangarakis, Gary P. Pelletier, and Marc S. Pepi

Technical Report MTL TR 91-27, July 1991, 14 pp- illus-tables, D/A Project: IL162105AH42

AD_____
UNCLASSIFIED
UNLIMITED DISTRIBUTION

Key Words

Metal matrix
Composites
Biaxial loading

Aluminum coupons reinforced unidirectionally with continuous alumina fibers were loaded in combined tension-torsion. Experimental results indicated that the superimposition of a 0.0025 shear strain reduced the tensile strain to failure by 67%. Similarly, the superimposition of a 0.0007 tensile strain reduced the shear strain to failure by 81%. It was inferred that applying the torque first and then the axial load or the axial load first and then the torque, had no significant effect on the failure envelope. The shear modulus was estimated to be 50.56 GPa.

U.S. Army Materials Technology Laboratory
Watertown, Massachusetts 02172-0001
RESPONSE OF AN ALUMINA FIBER REINFORCED ALUMINUM COMPOSITE TO COMBINED TENSION-TORSION -
Nikos Tsangarakis, Gary P. Pelletier, and Marc S. Pepi

Technical Report MTL TR 91-27, July 1991, 14 pp- illus-tables, D/A Project: IL162105AH42

AD_____
UNCLASSIFIED
UNLIMITED DISTRIBUTION

Key Words

Metal matrix
Composites
Biaxial loading

Aluminum coupons reinforced unidirectionally with continuous alumina fibers were loaded in combined tension-torsion. Experimental results indicated that the superimposition of a 0.0025 shear strain reduced the tensile strain to failure by 67%. Similarly, the superimposition of a 0.0007 tensile strain reduced the shear strain to failure by 81%. It was inferred that applying the torque first and then the axial load or the axial load first and then the torque, had no significant effect on the failure envelope. The shear modulus was estimated to be 50.56 GPa.

U.S. Army Materials Technology Laboratory
Watertown, Massachusetts 02172-0001
RESPONSE OF AN ALUMINA FIBER REINFORCED ALUMINUM COMPOSITE TO COMBINED TENSION-TORSION -
Nikos Tsangarakis, Gary P. Pelletier, and Marc S. Pepi

Technical Report MTL TR 91-27, July 1991, 14 pp- illus-tables, D/A Project: IL162105AH42

AD_____
UNCLASSIFIED
UNLIMITED DISTRIBUTION

Key Words

Metal matrix
Composites
Biaxial loading

Aluminum coupons reinforced unidirectionally with continuous alumina fibers were loaded in combined tension-torsion. Experimental results indicated that the superimposition of a 0.0025 shear strain reduced the tensile strain to failure by 67%. Similarly, the superimposition of a 0.0007 tensile strain reduced the shear strain to failure by 81%. It was inferred that applying the torque first and then the axial load or the axial load first and then the torque, had no significant effect on the failure envelope. The shear modulus was estimated to be 50.56 GPa.

U.S. Army Materials Technology Laboratory
Watertown, Massachusetts 02172-0001
RESPONSE OF AN ALUMINA FIBER REINFORCED ALUMINUM COMPOSITE TO COMBINED TENSION-TORSION -
Nikos Tsangarakis, Gary P. Pelletier, and Marc S. Pepi

Technical Report MTL TR 91-27, July 1991, 14 pp- illus-tables, D/A Project: IL162105AH42

AD_____
UNCLASSIFIED
UNLIMITED DISTRIBUTION

Key Words

Metal matrix
Composites
Biaxial loading

Aluminum coupons reinforced unidirectionally with continuous alumina fibers were loaded in combined tension-torsion. Experimental results indicated that the superimposition of a 0.0025 shear strain reduced the tensile strain to failure by 67%. Similarly, the superimposition of a 0.0007 tensile strain reduced the shear strain to failure by 81%. It was inferred that applying the torque first and then the axial load or the axial load first and then the torque, had no significant effect on the failure envelope. The shear modulus was estimated to be 50.56 GPa.